Alignment and rotation of spheroids in unsteady vortex flow

R. Jayaram [1], Y. Jie [2], J. J. J. Gillissen [3], L. Zhao [2], and H. I. Andersson [1]

[1]*Department of Energy and Process Engineering, Norwegian University of Science and Technology, 7491Trondheim, Norway*

[2]*AML, Department of Engineering Mechanics, Tsinghua University, Beijing 100084, China*

[3]*Department of Mathematics, University College London, Gower Street, WC1E 6BT, United Kingdom*

Preferential orientations of inertialess non-spherical particles are examined through three qualitatively different stages of a time-evolving Taylor-Green vortex flow. Despite an unexpected decorrelation between the vorticity vector and the direction of Lagrangian stretching, experienced by material fluid elements over a substantial time interval, prolate spheroids aligned with the Lagrangian stretching direction, whereas oblate spheroids aligned with the Lagrangian compression direction. We therefore infer that spheroidal tracers orient themselves relative to the Lagrangian history of the velocity gradients, defined by the left Cauchy-Green deformation tensor, rather than with the fluid vorticity vector. This preferential alignment persists all throughout the statistically unsteady flow field, and even in the inviscid and non-turbulent early stage of the time-dependent vortex flow. This explains the observed preferential spinning of rods and tumbling of disks, similarly as in homogeneous isotropic turbulence, even at the early stage when the flow is anisotropic and laminar. These preferred modes of particle rotation prevail all through the evolving flow, despite a surprisingly long time interval, during which the fluid vorticity decorrelates from the direction of Lagrangian stretching.

INTRODUCTION

The presence of small non-spherical particles in a viscous fluid can be observed in both industrial processes and in our environment [1]. Notable examples are pulp- and paper-making, combustion systems, ice crystals in clouds, marine snow, and transport of plankton in the ocean. How and why the particle orientates are of major concern. Particle orientation, for instance, influences the settling of tiny ice crystals in clouds, thereby affecting their collision and aggregation rates [2, 3]. Similarly, the ability of plankton to feed and reproduce is affected not only by oceanic turbulence but also by their shape through natural selection [4].

Particles without inertia passively follow the translational fluid motion, but unlike spheres, non-spherical tracers do not rotate passively with the fluid vorticity. The particle shape influences the orientation by preferential alignment relative to the local velocity gradient tensor in different flow systems, like in Homogeneous Isotropic Turbulence (HIT) [5] and turbulent channel flow [6]. These tendencies were recently associated with deformations of Lagrangian fluid elements. The

preferential alignment of rods and disks with Lagrangian stretching and compression directions, respectively, was first reported in HIT [7] and subsequently in wall turbulence [8, 9]. Computational [10, 11] and experimental [12, 13] studies have confirmed the role of the preferential alignment on the rotational particle behavior, such as spinning of rods and tumbling of disks.

The intricate behavior of non-spherical particles in three-dimensional flow fields has been studied in HIT [5, 7, 10] as well as in wall turbulence [6, 9, 14]. These studies have all been carried out in statistically steady flow fields. Particle velocity and acceleration statistics were recently studied in a statistically steady forced Taylor-Green flow [15]. The statistically *unsteady* Taylor-Green vortex (TGV) flow offers a different and unique environment where the orientation and rotation of non-spherical particles can be explored in an evolving flow field, in which the characteristic length and time scales vary continuously in time. An open question is how different, as compared to the already known behavior in HIT, tracer spheroids orient and rotate in the statistically developing TGV flow, especially in the earliest laminar stage of the evolving flow.

The TGV flow represents a relatively simple system, in which an initially smooth and anisotropic array of regular large-scale vortices evolves through a sequence of different flow stages. The essentially inviscid laminar flow in the earliest stage is subjected to vortex stretching and period-doubling [16, 17, 18], which gradually produce smaller flow structures and enhance the viscous energy dissipation. The accompanying enhancement of the enstrophy represents a measure of the strength of the vortex stretching [17] and reaches a maximum at a Reynolds-number dependent time t_{max}. The subsequent reduction of kinetic energy and enstrophy reflects the overall decay of the flow by viscous damping [17].

The unsteady TGV flow constitutes an attractive vehicle for assessment of the behavior of non-spherical particles in a *statistically unsteady* flow field. The continuously evolving vortex flow is distinctly different from the frequently studied channel-flow turbulence and HIT. We aim to explore how non-spherical particles orientate and rotate in the three-dimensional vortex field with the view to address the following questions: Do spheroidal particles orient preferentially in the evolving TGV flow? Do preferential spinning and tumbling, as known from isotropic turbulence, also occur in the anisotropic non-turbulent flow in the early laminar stage of the TGV-flow? Can it be that the fluid vorticity does not align with the Lagrangian stretching direction of the fluid elements through all stages of the evolving TGV flow? And, if so, can any preferential particle orientations be associated with Lagrangian coherent structures [7] even in an unsteady flow field where the fluid vorticity not necessarily orients with the Lagrangian stretching direction? The answers to these questions are of uttermost importance since any preferred particle orientation is believed to have a deciding influence on the particle rotation.

In this paper, we examine the behavior of inertialess spheroids in an evolving TGV flow through three qualitatively different stages of the flow. We focus on how particle shape, both oblate and prolate, affects the rate of particle rotation as well as the particle's rotation mode. To this end we also explore if and how tracer spheroids align themselves relative to the Lagrangian stretching and compression directions of the evolving flow field.

METHODOLOGY

The evolving TGV flow has proved successful for testing of numerical and perturbation methods for solving the time-dependent Navier-Stokes equations [16, 19, 20]. An unsteady TGV flow is realized in a Direct Numerical Simulation (DNS) where the incompressible Navier-Stokes equations are solved in a cubical box with sides $2\pi L$ and with periodic boundary conditions in all three coordinate directions. The three-dimensional flow field illustrated in Fig. 1(a) evolves from the two-dimensional initial field $u = V_0 \sin\left(\frac{x}{L}\right)\cos\left(\frac{y}{L}\right)\cos\left(\frac{z}{L}\right)$, $v = 0$, and $w = -V_0\cos\left(\frac{x}{L}\right)\cos\left(\frac{y}{L}\right)\sin\left(\frac{z}{L}\right)$, where V_0 and L are the initial velocity and length scales, respectively. The Reynolds number $Re = V_0 L/\nu = 1600$, where ν denotes the kinematic viscosity of the fluid. The numerical solution algorithm is described in Refs [21, 22]. The preceding analysis of clustering of inertial spheres by Jayaram et al. [22] was based on a simulation with 128^3 grid points, whereas the current simulation of inertialess spheroids uses 256×256×512 grid points. Pseudo-spectral integrations are performed in two of the coordinate directions. Twice as many grid points are used in the z-direction to compensate for the lower accuracy of the second-order finite-difference discretization in that direction.

Swarms of 2×10^6 non-interacting and passive spheroids with some different aspect ratios λ, are injected at random positions with random orientations at $t = 0$ and tracked using the same Lagrangian approach as in our earlier studies [8, 23]. The point-particle treatment is justified since the particle dimensions are smaller than the smallest length scales of the flow. When particle inertia is absent or negligibly small, the tracer spheroids translate with the local fluid velocity while experiencing zero force, and they rotate with zero torque due to the non-zero elements of the strain-rate tensor. With the Jeffery-torques [24] equated to zero, the particle rotation vector $\boldsymbol{\omega}'$ becomes $\omega_x' = -\Lambda S_{yz}' + \Omega_x'/2$, $\omega_y' = \Lambda S_{xz}' + \Omega_x'/2$, and $\omega_z' = \Omega_z'/2$. Here, $\Omega_i'/2$ is the fluid rotation-rate vector and S_{ij}' is the fluid strain-rate tensor in the particle frame of reference $x_i' = < x', y', z' >$, with origin at the particle center of mass; see Fig. 1(b). The shape factor $\Lambda = (\lambda^2 - 1)/(\lambda^2 + 1)$ measures the degree of asphericity of the prolate ($\lambda > 1$) and oblate ($\lambda < 1$) spheroids. Note that spherical tracers ($\lambda = 1$, $\Lambda = 0$) adapt to the fluid rotation.

We speculate that inertialess spheroids might align with the stretching or compression directions of material fluid elements also in the non-turbulent but unsteady stages of the evolving TGV-flow. To this end we follow Ni et al. [7] and compute the three eigenvectors (e_{L1}, e_{L2}, e_{L3}) of the left Cauchy-Green strain tensor $CG_{ij}^L = F_{ik}F_{jk}$, where F_{ij} denotes the deformation gradient tensor. The time evolution of F_{ij} is obtained by integrating $dF_{ij}/dt = A_{ik}F_{kj}(t)$, where A_{ik} is the instantaneous velocity gradient, along Lagrangian trajectories with initial condition $F_{ij}(t_0) = \delta_{ij}$; see [7, 8] for details.

As demonstrated by Ni et al. [7], the deformation gradient tensor $\boldsymbol{F}$ can be decomposed as $\boldsymbol{F} = \boldsymbol{VR}$, where $\boldsymbol{V}$ is the left stretch tensor and $\boldsymbol{R}$ is an orthogonal rotation tensor, representing the rigid-body rotation of the fluid element. Therefore, the left Cauchy-Green tensor is expressed as $\boldsymbol{CG^L} = \boldsymbol{FF^T} = \boldsymbol{VRR^TV^T} = \boldsymbol{V^2}$. The rotation tensor $\boldsymbol{R}$ is excluded in $\boldsymbol{CG^L}$, which only represents the

stretching properties of the fluid elements through the tensor $\boldsymbol{V}$. We are thus able to utilize the left Cauchy-Green tensor $\boldsymbol{CG}^L$, to examine particle alignments relative to the directions of local fluid stretching/compression in a Lagrangian approach. This approach provides information about how efficiently prolate and oblate spheroids respond to Lagrangian deformations of the local fluid elements, as already utilized to explain particle alignment in HIT and turbulent channel flow by Ni et al. [7] and Zhao & Andersson [8]., respectively.

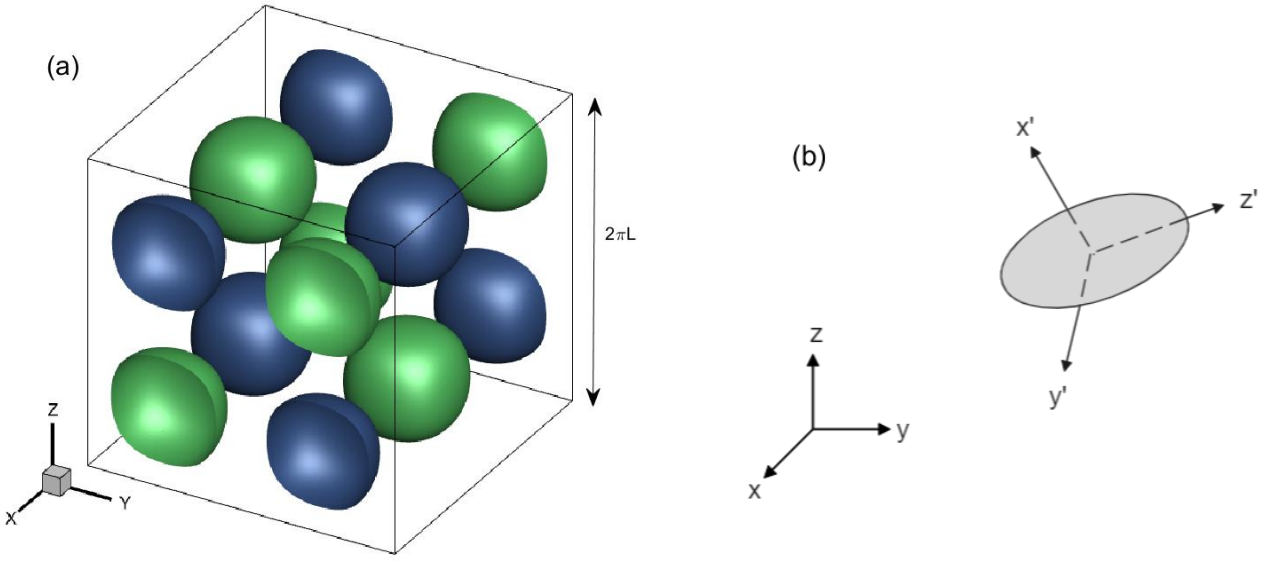

Figure 1: (a) The initial flow field in the cubical domain visualized by means of Ω_x where the two different colors distinguish between positive and negative values of Ω_x; (b) Illustration of the particle frame $x_i' = < x', y', z' >$ with its origin in the center of a prolate spheroid together with the inertial frame $x_i = < x, y, z >$ in which the DNS is performed. Note that the z'-direction is along the symmetry axis of the spheroid.

RESULTS AND DISCUSSION

A. Evolving Taylor-Green vortex (TGV) flow

The TGV flow is characterized by the time evolution of the volume-averaged kinetic energy E_k and viscous energy dissipation rate ϵ. While E_k decays monotonically in time, ϵ first exhibits a substantial increase until time $t = t_{max} \approx 9L/V_0$, from when a monotonic decay sets in [16, 18, 20, 22]. The energy dissipation rate ϵ shown in Figure 2(a) compares favorably with DNS data of Dairay et al. [19] at exactly the same Reynolds number. The volume-averaged enstrophy $\langle \zeta \rangle$, where $\zeta = \boldsymbol{\Omega} \cdot \boldsymbol{\Omega}$ is a scalar measure of the strength of the local vorticity vector $\boldsymbol{\Omega}$, is seen to overlap with ϵ. Although the viscous dissipation rate is locally different from the enstrophy, volume-averaging over a homogeneous flow domain gives that $\varepsilon = 2\nu\langle \zeta \rangle$ [25].

The initial flow field is essentially inviscid and the large-scale Taylor-Green vortices remain almost two-componential during the first stage of the flow development dominated by advection $(\boldsymbol{u}\cdot\nabla)\boldsymbol{\Omega}$ and stretching $(\boldsymbol{\Omega}\cdot\nabla)\boldsymbol{u}$ of vorticity [18]. Non-linear vortex stretching $\Omega_j\,\partial u_i/\partial x_j$ $(i=j)$ becomes increasingly important from time $t\approx 3L/V_0$ and the stretching of vortex lines gives rise to smaller-scale flow structures and therefore also to increasing dissipation ϵ. At the same time, the regular vortices in the earliest stage begin to deform as a result of bending of vortex lines through the non-linear term $\Omega_j\,\partial u_i/\partial x_j$ $(i\neq j)$ in the vorticity equation which transfers vorticity from the x_j to the x_i-direction.

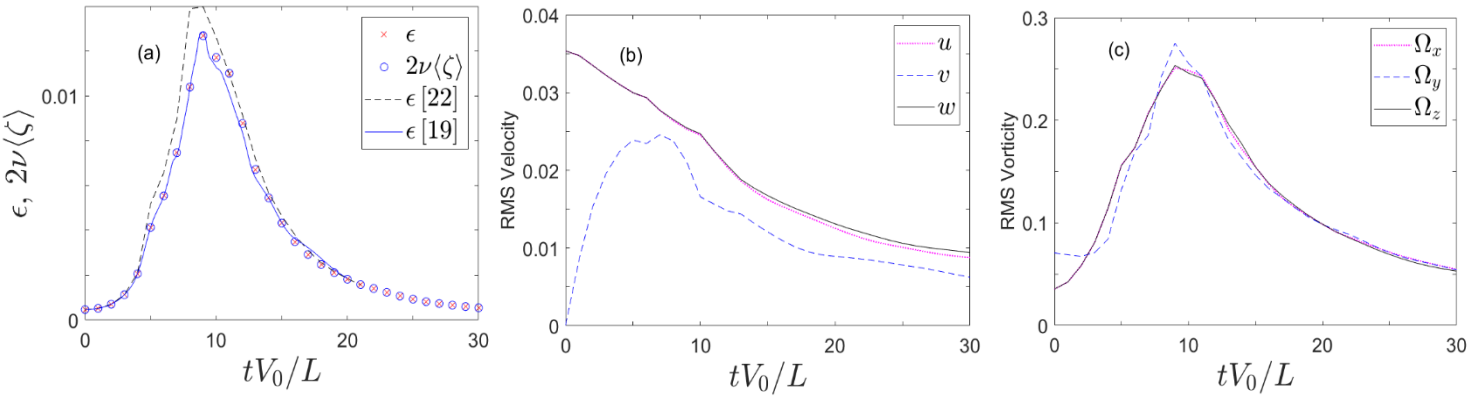

Figure 2: Time evolution of the TGV flow. (a) Viscous energy dissipation rate ϵ and enstrophy ζ, (b) RMS of velocity components u_i and (c) RMS of vorticity components Ω_i. The red cross and black dashed line in (a) denote the dissipation ϵ obtained with the present mesh and the coarser mesh [22], respectively, compared with ϵ (blue line) found by Dairay et al. [19]. The blue circles are volume-averaged enstrophy $\langle\,\zeta\,\rangle$.

The vorticity field Ω_i soon becomes isotropic, as shown in Figure 2(c). The velocity field u_i in Figure 2(b), however, gradually tends towards isotropy until the energy dissipation and the enstrophy peak at time $t\approx t_{max}$, but still remains somewhat anisotropic throughout the entire simulation. The early isotropization of the vorticity field is a result of vortex-tilting and consistent with the idea of a local equilibrium of the small-scale eddies [16]. The remaining coherence of the quasi-isotropic flow breaks down along with the gradually decaying enstrophy [18, 20, 22], thereby suggesting a resemblance with decaying HIT.

Figure 3 shows how the fluid vorticity vector $\boldsymbol{\Omega}$ aligns with the three eigenvectors $\boldsymbol{e}_{Li}$ of the left Cauchy-Green strain tensor CG^L. The vorticity immediately starts to align with the strongest Lagrangian stretching direction $\boldsymbol{e}_{L1}$ and their correlation soon exceeds the plateau level 0.6 obtained in HIT [7] and 0.57 in the almost isotropic center of a turbulent channel flow [8]. This finding suggests that this early stage of the flow is dominated by intense vortex stretching even though the flow field remains laminar [18, 26]. Contrary to the earlier studies, in which the correlation $\langle(\boldsymbol{e}_{L1}\cdot\boldsymbol{\Omega})^2\rangle$ monotonically increased until it saturated at a certain level, the present alignment first increases and then experiences a modest decline after time $t\approx 3L/V_0$. This

unexpected behavior is clearly associated with major structural reorganizations of the flow field, evidenced by the growth of enstrophy and viscous energy dissipation seen in Figure 2(a), associated with period-doubling, vortex stretching and bending [18]. The slight decorrelation between $\boldsymbol{\Omega}$ and $\boldsymbol{e}_{L1}$ persists for about $10L/V_0$, thereafter the vorticity once again exhibits a slight increasing alignment with the Lagrangian stretching direction. The weakly resuming correlation from time $t \approx 14L/V_0$ somehow resembles the time evolution of the alignment reported in statistically steady HIT [7] and seems to saturate at $\langle(\boldsymbol{e}_{L1} \cdot \boldsymbol{\Omega})^2\rangle \approx 0.55$ after $20L/V_0$. Just as in HIT, this plateau arises when a dynamic balance between vortex stretching and viscous dissipation has been established.

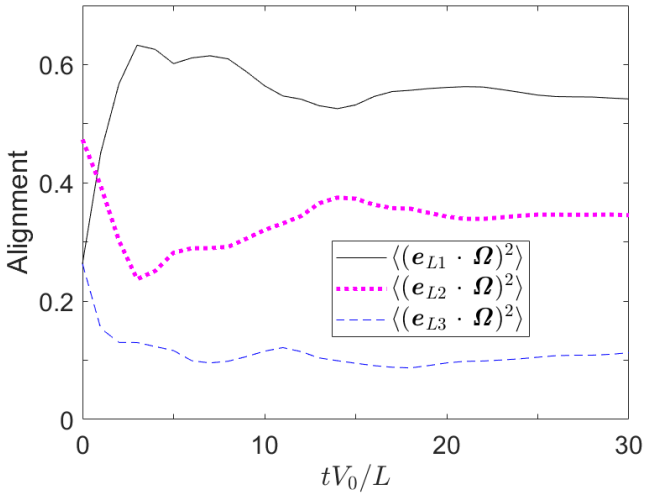

Figure 3: Time evolution of the alignment of fluid vorticity $\boldsymbol{\Omega}$ relative to the three eigenvectors $\boldsymbol{e}_{Li}$ of the left Cauchy-Green strain tensor. Here, $\boldsymbol{e}_{L1}$ and $\boldsymbol{e}_{L3}$ are the maximum (stretching) and minimum (compression) eigenvectors, respectively, obtained by integrating from $t_0 = 0$. The correlations $(\boldsymbol{e}_{Li} \cdot \boldsymbol{\Omega})^2$ are first evaluated at the particle positions and subsequently averaged over all particles in the cubical volume shown in Figure 1(a).

B. Particle orientation and rotation

The particle enstrophy, defined as the mean square rotation rate $\langle\omega_i\omega_i\rangle$, exhibits a non-monotonic time evolution similarly as that of the fluid enstrophy $\langle\, \zeta \,\rangle$ in Figure 2(a). However, shape has only a modest effect on the particle enstrophy in Figure 4(c). Nevertheless, shape has a considerable influence on the mode of rotation, i.e. whether the spheroidal particle spins about its symmetry axis (z') or tumbles about the two other axes $(x' \text{and } y')$. We observe from Figure 4(a) that disks tumble more than rods, whereas Figure 4(b) shows that rods spin more than disks. The preferential tumbling of disks and spinning of rods have been reported before in studies of statistically steady HIT [5, 10, 11, 27]. Now, although only the TGV flow field from $t \approx 15L/V_0$ and onwards resembles HIT, these preferred modes of rotation remain the same through all stages of the flow development, even at the still essentially inviscid and anisotropic early stage $t = 3L/V_0$. The results in Figure 4 also suggest that spinning is more shape-dependent than tumbling. It is furthermore

interesting to observe that aspherical particles ($\lambda \neq 1$) exhibit a somewhat lower rotation rate than spheres in the early stage of the flow evolution, whereas aspherical particles rotate faster than spheres at $t = t_{max} \approx 9L/V_0$. This peculiar phenomenon is caused by the fluid strain-rate S'_{ij}, which is the only means that makes inertialess spheroids ($\lambda \neq 1$) rotate differently than tracer spheres ($\lambda = 1$).

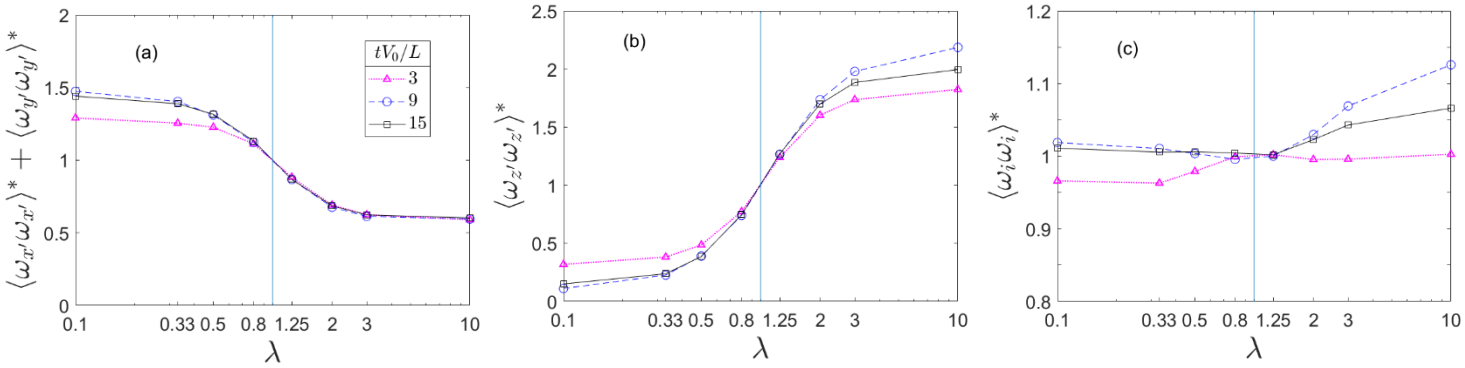

Figure 4: (a) Tumbling $\langle\omega_{x'}\omega_{x'}\rangle + \langle\omega_{y'}\omega_{y'}\rangle$, (b) spinning $\langle\omega_{z'}\omega_{z'}\rangle$, and (c) total particle enstrophy versus aspect ratio λ at three different stages of the flow development. Star quantities are normalized by the corresponding values for spheres ($\lambda = 1$).

Understanding how particle shape affects the rotation modes, as observed in Figure 4, requires examination of the particle orientation angle α relative to the fluid vorticity, where $\cos\alpha$ is obtained from the dot product between the particle orientation unit vector $\boldsymbol{p}$, aligned with its symmetry axis, and the local fluid vorticity vector $\boldsymbol{\Omega}$ [6]. Figure 5 shows that disks tend to align orthogonally to the fluid vorticity, which causes strong tumbling [6, 10]. In striking contrast to disks, rods are strongly aligned with the local vorticity and thus spin along with it. These alignment effects are consistently largest for spheroids with maximum deviation from sphericity. Surprisingly, similar alignments as those observed at the early stage $t = 3L/V_0$ (fig. 5(a)) of the flow development are also observed much later at $t = 9L/V_0$ (fig. 5(b)), although the flow field has undergone dramatic changes in between. This indicates that the large-scale and almost inviscid cellular vortex structures prevailing at the early stage of the evolving TGV flow orient the spheroids similarly as the turbulent-like smaller-scale vortices at later stages. This also explains why shape has qualitatively the same effects on the particle rotation mode through the different stages of the flow development. It is noteworthy that similar particle alignments with the fluid vorticity persists all through the evolving TGV flow, i.e. not only in the later turbulence-like regime, but also at the early laminar stage. A deeper insight in the underlying alignment mechanisms will now be sought by means of an analysis of Lagrangian deformations of the fluid elements.

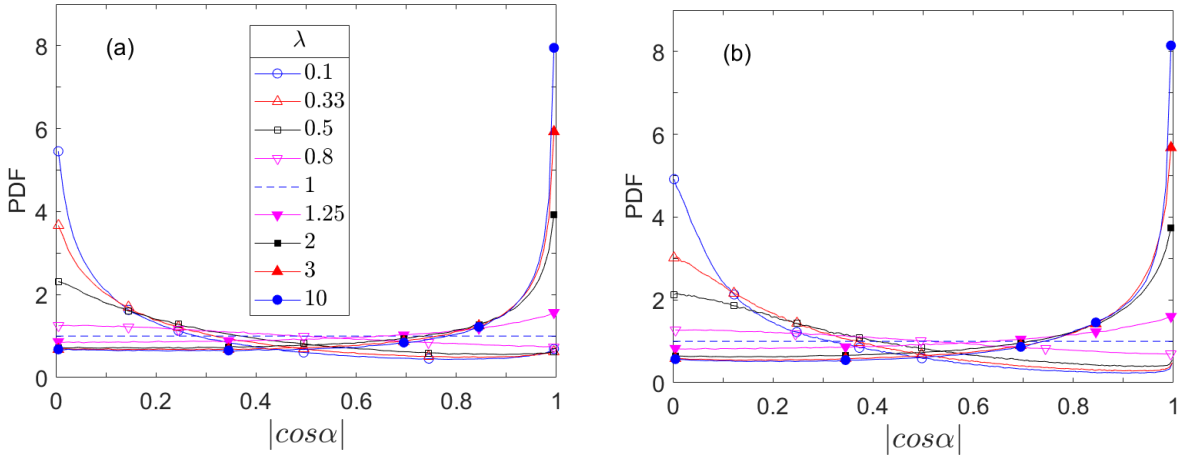

Figure 5: Probability density function of the direction cosine of the alignment α of a spheroid with the local fluid vorticity. (a) $t = 3L/V_0$; (b) $t = 9L/V_0$. The broken line represents randomized alignment of spherical particles ($\lambda = 1$).

The time histories of the alignment of the particle orientation $\boldsymbol{p}$ with the three eigenvectors $\boldsymbol{e}_{Li}$ of the left Cauchy-Green strain tensor are presented in Figure 6 for flat disks ($\lambda = 0.1$) and long rods ($\lambda = 10$). The usefulness of correlations such as $\langle(\boldsymbol{e}_{Li} \cdot \boldsymbol{p})^2\rangle$ is appropriate only for particles with relatively large asphericity [7], such as the flat disks and the long rods examined in Figure 6. The long rods in Fig. 6(b) preferentially align with the maximum Lagrangian eigenvector $\boldsymbol{e}_{L1}$, i.e. in the extensional or stretching direction. The correlation $\langle(\boldsymbol{e}_{L1} \cdot \boldsymbol{p})^2\rangle$ increases monotonically in time and tends to unity, similarly as for long rods in HIT [7] and turbulent channel flow [8]. This contrasts, however, with the observed decorrelation between $\boldsymbol{e}_{L1}$ and $\boldsymbol{\Omega}$, which sets in at $t \approx 3L/V_0$ and persists until time t about $14L/V_0$, as seen in Figure 3. The almost negligible influence of the fluid viscosity during the early stage of the flow development makes the stretching of vorticity indistinguishable from the stretching of Lagrangian fluid lines [18, 26]. This explains the strong alignment of rods with both the Lagrangian stretching direction $\boldsymbol{e}_{L1}$ and with the vorticity vector $\boldsymbol{\Omega}$ at $t \approx 3L/V_0$. Although the flow field undoubtedly remains laminar, the latter alignment gives rise to the rapid spinning of long rods seen in Fig. 4(b).

A further enhanced spinning of rods is observed at $t \approx t_{max} = 9L/V_0$, but this cannot be ascribed to a better unconditioned alignment $\langle(\boldsymbol{e}_{L1} \cdot \boldsymbol{\Omega})^2\rangle$. By conditioning on vorticity magnitude, however, Ni et al. [7] showed that stronger vorticity is better aligned with the largest Lagrangian stretching direction. Accordingly, we believe that the rapid spinning of rods at time t_{max} is caused by the tenfold increase of enstrophy $\langle \zeta \rangle$.

The alignment trends of rods with $\boldsymbol{e}_{L1}$ continue throughout the time span during which $\boldsymbol{\Omega}$ decorrelates from $\boldsymbol{e}_{L1}$. This can only be explained by the emerging influence of viscosity, which makes the fluid vorticity evolve differently than Lagrangian fluid line elements, which

asymptotically align in the direction of Lagrangian fluid stretching. Dynamically, this de-alignment between $\boldsymbol{p}$ and $\boldsymbol{\Omega}$ reduces the spinning rate of the long rods at $t = 15L/V_0$. Thereafter, however, the alignment $\langle(\boldsymbol{e}_{L1} \cdot \boldsymbol{\Omega})^2\rangle$ persists, which implies that the rod-like particles maintain their orientation along the vorticity vector $\boldsymbol{\Omega}$, which in turn promotes preferential particle spinning, similarly as in statistically steady HIT [7] and channel flow turbulence [8].

Flat disks, on the other hand, preferentially align with the Lagrangian compression direction $\boldsymbol{e}_{L3}$ all through the flow development, analogously to observations in wall turbulence [8]. The vorticity vector $\boldsymbol{\Omega}$, however, rapidly de-aligns with $\boldsymbol{e}_{L3}$ and the correlation $\langle(\boldsymbol{e}_{L3} \cdot \boldsymbol{\Omega})^2\rangle$ in Fig. 3 eventually decays almost to zero. The inferred orthogonality between disks and the vorticity makes disks tumble rather than spin. The essentially monotonic de-alignment $\langle(\boldsymbol{e}_{L3} \cdot \boldsymbol{\Omega})^2\rangle$ in Figure 3 contrasts with the non-monotonous alignment $\langle(\boldsymbol{e}_{L1} \cdot \boldsymbol{\Omega})^2\rangle$. This suggests that the orthogonality between disks and vorticity is more modestly affected by the flow development. Indeed, the tumbling rate of disk-like particles remains almost constant after time $t \approx t_{max} = 9L/V_0$ in Figure 4(a).

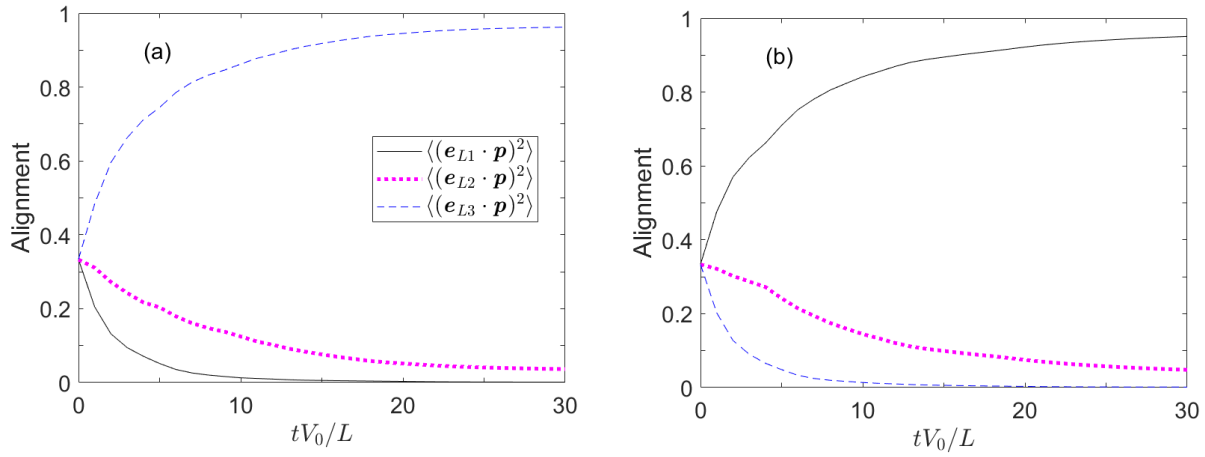

Figure 6: Time histories of the alignment $\langle(\boldsymbol{e}_{Li} \cdot \boldsymbol{p})^2\rangle$ of the orientation vector $\boldsymbol{p}$ of spheroidal particles relative to the three eigenvectors $\boldsymbol{e}_{Li}$ of the left Cauchy-Green strain tensor. (a): Flat disks, $\lambda = 0.1$ (b): Long rods, $\lambda = 10$.

CONCLUDING REMARKS

From simulations of particle-laden Taylor-Green vortex flow, we have demonstrated that the evolving three-dimensional flow field constitute a new vehicle for explorations of particle additives in vortical flows. The early advection-dominated TGV flow transits through qualitatively different stages, first when non-linear vortex stretching and bending sets in, and later when viscous action comes into play. This gave rise to an unexpected decorrelation between vorticity $\boldsymbol{\Omega}$ and the Lagrangian stretching direction $\boldsymbol{e}_{L1}$ over a $10L/V_0$ time interval. Such decorrelations have not been observed before in statistically steady flow fields, neither in HIT [7] nor in wall turbulence [8].

We ascribe this phenomenon to an increasing influence of viscous action as the unsteady TGV flow evolves in time.

We found that inertialess spheroids rotate in the three-dimensional vortex flow similarly as in HIT, even though the early and essentially inviscid stage of the TGV flow is laminar rather than turbulent. Nevertheless, prolate and oblate spheroids preferentially spin and tumble, respectively. These preferred modes of rotation persist all through the flow development, despite the substantial time interval during which the vorticity decorrelates with the Lagrangian stretching direction. Nevertheless, prolate and oblate spheroids persistently align in the stretching $\boldsymbol{e}_{L1}$ and compression $\boldsymbol{e}_{L3}$ directions, respectively, all through the qualitatively different stages of the simulation. Contrary to in steady HIT, in which rods and vorticity independently align with $\boldsymbol{e}_{L1}$ and therefore with each other [5, 7], prolate spheroids preferentially align with $\boldsymbol{e}_{L1}$ even though they unexpectedly de-align with $\boldsymbol{\Omega}$ during a substantial period of the flow development. Finally, the present results give further support to the hypothesized [7, 8] universality of preferential alignment of rods and disks with the Lagrangian stretching and compression directions, respectively. Herein, the preference is demonstrated to apply also in the inviscid and non-turbulent stage of the evolving TGV-flow.

The evolving TGV flow has enabled us to investigate the preferential alignment and the accompanying modes of rotation of inertialess spheroids through the qualitatively different stages of the flow. Inertialess particles distribute themselves evenly throughout the flow field, whereas inertial particles are known to concentrate preferentially, as already shown for inertial spheres by Jayaram et al. [22]. Particle inertia is moreover known to make spheroidal particles orient and rotate completely different from tracer spheroids with the same aspect ratio λ; see e.g. Zhao et al. [6, 14]. The conclusions drawn from the present investigation of inertialess spheroids are therefore not valid for inertial particles, unless the particle inertia is negligibly small, i.e. unless the effective Stokes number is well below unity.

The present analysis of preferential orientation of inertialess spheroids benefited from the usage of the Lagrangian deformation directions of the local fluid elements, as deduced from the left Cauchy-Green tensor. This approach can be further extended to include also the solid-body rotation of the eigenvectors of the Cauchy-Green tensor. In that way, we believe that the rotation of the eigenvectors can be associated with particle rotation. It should anyhow be recalled that the Cauchy-Green tensor-based approach to study particle alignments has been restricted to inertialess particles [7, 8], for which the trajectories of the tracer particles coincide with the trajectories of the infinitesimal fluid elements. The trajectory of an inertial particle, however, will inevitably depart from the path followed by an initially co-located fluid element and thereby prohibit straightforward computations of such correlations as shown in Figure 6.

ACKNOWLEDGEMENTS

The authors acknowledge support by the Research Council of Norway through Grant Nos. 250744 and NN2694K and from the Natural Science Foundation of China through Grant Nos. 11702158 and 91752205. Professor Eric Lamballais kindly provided the DNS data from Ref. [19] plotted in Figure 2(a).

DATA AVAILABILITY STATEMENT

The data that support the findings of this study are available from the corresponding author upon reasonable request.

REFERENCES

[1] G. A. Voth and A. Soldati, Anisotropic particles in turbulence, Annu. Rev. Fluid Mech. **49**, 249 (2017).

[2] C. Siewert, R. P. J. Kunnen, and W. Schröder, Collision rates of small ellipsoids settling in turbulence, J. Fluid Mech. **758**, 686–701 (2014).

[3] J. Jucha, A. Naso, E. Lévêque, and A. Pumir, Settling and collision between small ice crystals in turbulent flows, Phys. Rev. Fluids **3**, 014604 (2018).

[4] G. Basterretxea, J. S. Font-Munoz, and I. Tuval, Phytoplankton orientation in a turbulent ocean: A microscale perspective, Front. Mar. Sci. **7** , 185 (2020).

[5] A. Pumir and M. Wilkinson, Orientation statistics of small particles in turbulence, New J. Phys. **13**, 093030 (2011).

[6] L. Zhao, N. R. Challabotla, H. I. Andersson, and E. A. Variano, Rotation of nonspherical particles in turbulent channel flow, Phys. Rev. Lett. **115**, 244501 (2015).

[7] R. Ni, N. T. Ouellette, and G. A. Voth, Alignment of vorticity and rods with Lagrangian fluid stretching in turbulence, J. Fluid Mech. **743**, R3 (2014).

[8] L. Zhao and H. I. Andersson, Why spheroids orient preferentially in near-wall turbulence, J. Fluid Mech. **807**, 221 (2016).

[9] K. Yang, L. Zhao, and H. I. Andersson, Mean shear versus orientation isotropy: effects on inertialess spheroids' rotation mode in wall turbulence, J. Fluid Mech. **844**, 796-816 (2018).

[10] S. Parsa, E. Calzavarini, F. Toschi, and G. A. Voth, Rotation rate of rods in turbulent fluid flow, Phys. Rev. Lett. **109**, 134501 (2012).

[11] M. Byron, J. Einarsson, K. Gustavsson, G. Voth, B. Mehlig, and E. A. Variano, Shape-dependence of particle rotation in isotropic turbulence, Phys. Fluids **27**, 035101 (2015).

[12] G. G. Marcus, S. Parsa, S. Kramel, R. Ni, and G. A. Voth, Measurements of the solid-body rotation of anisotropic particles in 3D turbulence, New J. Phys. **16 (10),** 102001 (2014).

[13] R. Ni, S. Kramel, N. T. Ouellette, and G. A. Voth, Measurements of the coupling between the tumbling of rods and the velocity gradient tensor in turbulence, J. Fluid Mech. **766**, 202 (2015).

[14] L. Zhao, N. R. Challabotla, H. I. Andersson, and E. A. Variano, Mapping spheroid rotation modes in turbulent channel flow: effects of shear, turbulence and particle inertia, J. Fluid Mech. **876**, 19 (2019).

[15] S. Angriman, P. D. Mininni, and P. J. Cobelli, Velocity and acceleration statistics in particle-laden turbulent swirling flows, Phys. Rev. Fluids **5**, 064605 (2020).

[16] S. A. Orszag, Numerical simulation of the Taylor-Green vortex, in Computing Methods in Applied Sciences and Engineering Part 2: International Symposium, Versailles (Springer, Berlin, Heidelberg), 50 (1974).

[17] M. E. Brachet, D. I. Meiron, S. A. Orszag, B. G. Nickel, R. H. Morf, and U. Frisch, Small-scale structure of the Taylor-Green vortex, J. Fluid Mech. **130**, 411-452 (1983).

[18] N. Sharma and T. K. Sengupta, Vorticity dynamics of the three-dimensional Taylor-Green vortex problem, Phys. Fluids **31**, 035106 (2019).

[19] T. Dairay, E. Lamballais, S. Laizet, and J. C. Vassilicos, Numerical dissipation vs subgrid-scale modelling for large eddy simulation, J. Comput. Phys. **337**, 252 (2017).

[20] J. R. DeBonis, Solutions of the Taylor-Green vortex problem using high-resolution explicit finite difference methods, AIAA 51^{st} Aerospace Sciences Meeting, Grapevine, Texas, AIAA-paper **0382** (2013).

[21] R. Jayaram, J. J. J. Gillissen, L. Zhao, and H. I. Andersson, Numerical solution of Poisson equation using Sherman-Morrison algorithm in Taylor-Green vortex flow, in Proceedings of 10^{th} National conference on Computational Mechanics, Trondheim, Norway (Centre Internacional de Mètodes Numèrics a l'Enginyeria, Barcelona, Spain), 197 - 210 (2019).

[22] R. Jayaram, Y. Jie, L. Zhao, and H. I. Andersson, Clustering of inertial spheres in evolving Taylor-Green vortex flow, Phys. Fluids **32**, 043306 (2020).

[23] N. R. Challabotla, L. Zhao, and H. I. Andersson, Shape effects on dynamics of inertiafree spheroids in wall turbulence, Phys. Fluids **27**, 061703 (2015).

[24] G.B. Jefferey, The motion of ellipsoidal particles immersed in a viscous fluid, Proc. R. Soc. Lond. A **102**, 161-179 (1922).

[25] D. A. Donzis, P. K. Yeung, and K. R. Sreenivasan, Dissipation and enstrophy in isotropic turbulence: Resolution effects and scaling in direct numerical simulations, Phys. Fluids **20**, 045108 (2008).

[26] N. Sharma, T. K. Sengupta, and J. R. Brinkerhoff, Non-linear instability analysis of the three -dimensional Navier-Stokes equations: Taylor-Green vortex problem, Phys. Fluids **32**, 064102 (2020).

[27] K. Gustavsson, J. Einarsson, and B. Mehlig, Tumbling of small axisymmetric particles in random and turbulent Flows, Phys. Rev. Lett. **112**, 014501 (2014).